Journal of
Synchrotron Radiation

ISSN 0909-0495

Received 4 September 2008
Accepted 24 April 2009

Short-term effects of synchrotron irradiation on vasculature and tissue in healthy mouse brain

Clément Ricard,[a,b] Manuel Fernández,[a,b] Jérôme Gastaldo,[a,b] Lucie Dupin,[a,b] Laurette Somveille,[a,b] Régine Farion,[a,b] Herwig Requardt,[c] Jean-Claude Vial,[d,b] Hélène Elleaume,[a,b] Christoph Segebarth[a,b] and Boudewijn van der Sanden[a,b]*

[a]INSERM, U836, Grenoble Institut des Neurosciences, F-38042 Grenoble, France, [b]Université Joseph Fourier, F-38041 Grenoble, France, [c]European Synchrotron Radiation Facility, Medical Beamline ID17, BP 220, F-38043 Grenoble, France, and [d]Laboratoire de Spectrométrie Physique, CNRS UMR 5588, F-38402 Grenoble, France. E-mail: boudewijn.vandersanden@ujf-grenoble.fr

The purpose of this study is to measure the effects of a tomographic synchrotron irradiation on healthy mouse brain. The cerebral cortexes of healthy nude mice were irradiated with a monochromatic synchrotron beam of 79 keV at a dose of 15 Gy in accordance with a protocol of photoactivation of cisplatin previously tested in our laboratory. Forty-eight hours, one week and one month after irradiation, the blood brain barrier (BBB) permeability was measured in the irradiated area with intravital multiphoton microscopy using fluorescent dyes with molecular weights of 4 and 70 kDa. Vascular parameters and gliosis were also assessed using quantitative immunohistochemistry. No extravasation of the fluorescent dyes was observed in the irradiated area at any measurement time (48 h, 1 week, 1 month). It appears that the BBB remains impermeable to molecules with a molecular weight of 4 kDa and above. The vascular density and vascular surface were unaffected by irradiation and no gliosis was induced. These findings suggest that a 15 Gy/79 keV synchrotron irradiation does not induce important damage on brain vasculature and tissue on the short term following irradiation.

Keywords: synchrotron radiotherapy; multiphoton microscopy; blood-brain-barrier permeability; healthy brain tissue and irradiation; gliosis.

1. Introduction

Brain tumors are amongst the most severe forms of cancer (DeAngelis, 2001). They are often lethal, even for benign tumors that develop malignancy over time. In the USA, brain tumors accounted for 1.4% of all cancers and for 2.4% of all cancer deaths in 2005 (Greenlee *et al.*, 2000). Glioblastoma multiforme (GBM) is the most aggressive among primary brain tumors (Behin *et al.*, 2003). Median survival time for patients bearing a GBM is less than one year, and five year survival rate is below 5% (Gurney & Kadan-Lottick, 2001).

Treatments aim at prolonging survival time. They include surgery, radiotherapy (Bernier *et al.*, 2004), chemotherapy (Muldoon *et al.*, 2007) and these approaches are often applied in combination (Stupp *et al.*, 2005; Van Tassel *et al.*, 1995; Mehta & Khuntia, 2005). Efficiency remains poor for several reasons: (i) tumor cells located in the immediate vicinity or infiltrated in vital functional areas are often not removed during surgery; (ii) chemotherapeutic drug delivery remains difficult as the interstitial tumor fluid pressure is high (Muldoon *et al.*, 2007); and (iii) radiotherapy is only intended to prolong survival, as the doses delivered are limited by the radiosensitivity of healthy brain tissue (Schultheiss *et al.*, 1995).

Radiotherapy of brain tumors can lead to various side effects (Schultheiss *et al.*, 1995). Whole-brain irradiation may lead to cognitive dysfunction in between months to years after treatment (Roman & Sperduto, 1995). Patients can even develop severe dementia after whole brain therapy (DeAngelis *et al.*, 1989). In rats, late radiation-induced injuries were also observed, such as a decline in cognitive function and morphological modifications, including demyelination, necrosis and gliosis (Akiyama *et al.*, 2001). Histological findings are similar to those observed in neurodegenerative diseases.

The use of modern imaging modalities such as MRI (magnetic resonance imaging), CT (computed tomography) or PET (positron emission tomography) has significantly improved tumor delineation. Hence it has become possible to maximize dose deposit inside the tumor while minimizing dose deposit in the surrounding healthy areas. Furthermore, radiosensitizers and dose-enhancing agents taken up by the tumor may help to improve the therapeutic efficacy of the treatment. This is the case of drugs such as cisplatin that can be

both a dose-enhancing agent when photoactivated by irradiation and a radiosensitizer when it blocks the activation of repair pathways (Turchi *et al.*, 2000).

Photoactivation therapy (PAT), a new kind of chemo-radiotherapy, has recently been developed at the European Synchrotron Radiation Facility (ESRF) in Grenoble. With this new method, the tumor volume is tomographically irradiated with kilovoltage X-rays one day after intratumoral injection of high-*Z* compounds, *e.g.* iodine (Adam *et al.*, 2003, 2006) or cisplatin (Biston *et al.*, 2004; Rousseau, Boudou, Barth *et al.*, 2007). In recent experiments on the F98 rat glioma model, the irradiation energy was set closely to the *K*-edge of platinum (78.39 keV) and the dose was 15 Gy ('PAT-Plat Protocol') (Biston *et al.*, 2004). Curative effects were observed in 30% of the treated animals (Biston *et al.*, 2004).

The next step was to demonstrate the minimal toxicity of the treatment for the healthy tissues surrounding the tumor. One of the first concerns was the neurotoxicity of the cisplatin. A lot of work was done in our group to determine the best way to deliver the cisplatin within the tumor. Convection-enhanced delivery (Rousseau, Boudou, Esteve *et al.*, 2007) as well as the use of osmotic pumps were investigated and it was demonstrated that the drug distribution is maximum within the lesion and is minimum in healthy adjacent tissues.

Following these successful results, phase I clinical trials are now in preparation at the ESRF. In the meantime, certain matters still need to be investigated at the preclinical level. One of them is the effects of synchrotron tomographic irradiation on healthy tissues. To cover the whole tumoral volume with our set-up and despite the use of a tomographic protocol, some parts of healthy tissues will have to be irradiated.

In this study on healthy mouse brain tissue, we determine potential side effects of the synchrotron irradiation applied in the PAT-Plat protocol. Cisplatin was not used in these experiments as the aim of our study was to investigate the effects of the irradiation on healthy brain tissue. BBB leakage, blood perfusion, vascular parameters and gliosis were assessed on normal nude mice in between 48 h and one month after irradiation. The rationale behind the choice of this animal model is that it enables *in vivo* two-photon microscopic imaging (Helmchen & Denk, 2005; Schenke-Layland *et al.*, 2006; König, 2000) of the brain without dura removal. In rats, the dura is not transparent and it needs to be removed for *in vivo* measurements. This intervention may induce physiological and hemodynamic changes that could interfere with the experiments.

2. Materials and methods

2.1. Animal care guidelines

All experimental procedures were performed in accordance with the French Government guidelines for care and use of laboratory animals (licenses no. 380702, A 3851610004 and B 3851610003). Female nude mice (Charles River Laboratories, France) were used in the experiments.

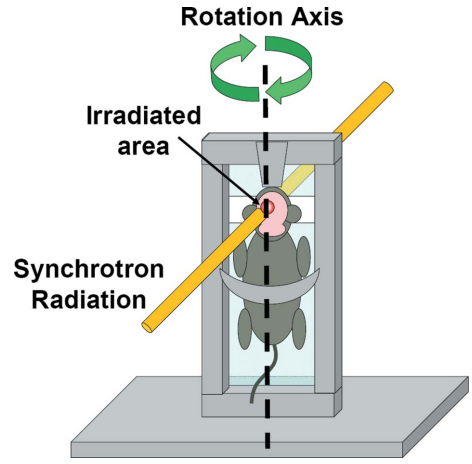

Figure 1
Irradiation set-up. Schematic representation of the positioning of the mouse on the stereotactic frame during synchrotron irradiation.

2.2. Irradiation procedure

2.2.1. Animal preparation. Animals were anaesthetized with an intraperitoneal injection of a mixture of 10 mg kg^{-1} xylazine and 100 mg kg^{-1} ketamine in a 0.9% NaCl saline solution. They were positioned in a custom-made vertical stereotactic frame which was fixed on a rotation and translation motorized stage. The rotation axis was oriented caudo-cranially and it crossed the cerebral cortex in the healthy animals (Fig. 1). The temperature of the animals was maintained at a physiological level during the whole experiment using heated gels.

2.2.2. ESRF source. A highly collimated and monochromatic synchrotron beam was used. The radiation source was a multipole wiggler situated 150 m upstream of the animal. Divergence of the source was 0.1 mrad vertically and about 3 mrad horizontally. Collimation slits were set to define a fan beam of 1.5 mm × 1.5 mm. The beam was monochromated at 79 keV, just above the absorption *K*-edge of platinum (78.39 keV). Monochromatization was achieved by means of a pair of bent silicon crystals in transmission (Laue) mode. Band-pass was approximately 80 eV.

Before each irradiation, a CT scan of the head of the animal was acquired. Images from this scan were used to define the irradiation volume. The animals were irradiated in tomographic mode with a beamwidth of 1.5 mm (irradiated volume 1.75 mm^3). The dose rate normalized to the electron current of the synchrotron storage ring was 9.9×10^{-4} Gy mA^{-1} s^{-1} at skin entrance. The device rotation speed was adjusted to deliver 15 Gy at the rotation axis. This dose had proven to have optimal PAT-Plat effects on rats bearing F98 glioma (Biston *et al.*, 2004).

2.3. Intravital two-photon microscopy

2.3.1. Animal preparation. At 48 h, one week and one month after the irradiation, mice (n = 5 per timepoint) were anaesthetized with a continuous inhalation of isoflurane (2%) in a gas mixture of O_2 and N_2O (30% and 70%, respectively).

The heads of the animals were immobilized in a stereotactic frame to minimize breathing movements. The temperature of the animals was monitored and maintained at 310 K using a warm water blanket. Craniotomy (3–4 mm in diameter) was performed above the irradiated cortex and a 0.9% NaCl solution was deposited in between the surface of the brain and the objective.

A cocktail of 100 µl of a 100 mg ml^{-1} RhodamineB-dextran 70 kDa solution and of 100 µl of a 100 mg ml^{-1} FITC-dextran 4 kDa solution (Sigma-Aldrich) in 0.9% NaCl was injected into the tail vein of the mouse approximately 10 min before the two-photon microscopy studies.

Fluorescence from the two dyes was observed in five parallel fields of view of the irradiated cortex that were located at a depth between 0 and 300 µm below the dura (Fig. 2). Controls were realised on healthy mice with or without mechanically induced BBB disruption. BBB disruption was induced by applying repeatedly local mechanical pressure at the surface of the cortex. The permeability of the BBB was assessed qualitatively by comparing the pixel intensity in regions of interest in the perfused vessels and in the extravascular space of control as well as in irradiated animals. The *in vivo* two-photon microscopic measurements are limited to the surface of the irradiated cortical volume. Therefore, additional quantitative immunohistochemical analyses of the vascular bed were necessary to gain a complete view of the irradiated volume (see below and Fig. 2).

2.3.2. Microscopy set-up. Two-photon laser confocal scanning microscopy was performed with a Biorad MRC 1024 scanhead and an Olympus BX50WI microscope. Fluorescence signals were directly epicollected. An 800 nm excitation beam from a Tsunami femtosecond Ti:sapphire laser (5 W pump; Spectra-Physics, Millenia V) was focused onto the surface of the brain using a 20× water-immersion objective (0.95 NA, Xlum Plan Fl Olympus).

The beam was scanned in the *xy* plane to acquire 512 × 512 pixel images in 0.9 s. The observation depth (*z*-scan) was varied by moving the motorized objective vertically. Incident laser intensity was adjusted by using a half-wave length plate and a polarizer placed before the microscope. The total average power delivered at the surface ranged from 1 to 150 mW. Two channels (red and green) could be simultaneously observed using two external photomultiplicator tubes (PMT) equipped with an appropriate set of filters [HQ 620/60 and 710 ASP in front of PMT1 (red channel); HQ 535/30 and BG39 in front of PMT2 (green channel)].

Images were acquired using the Biorad exploitation system and they were displayed using *ImageJ* software (version 1.33 public domain software, available from http://rsb.info.nih.gov/ij/).

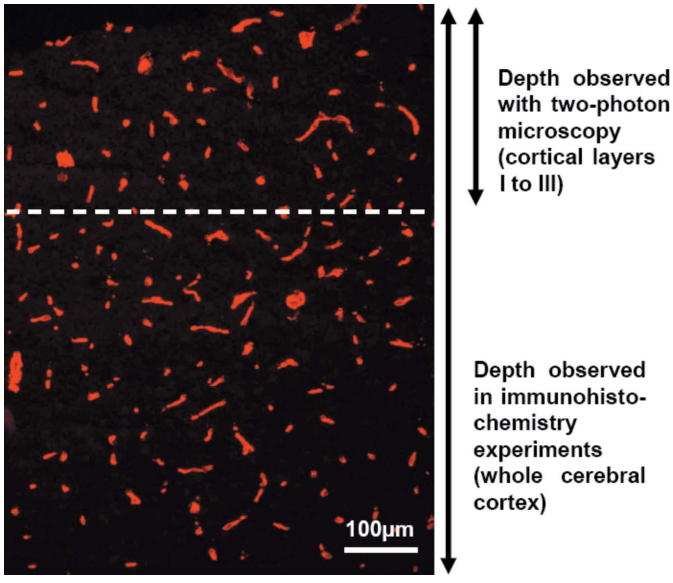

Figure 2
Two-photon microscopy *versus* immunohistochemistry fields of view. Immuno-labelling of the collagen IV in basal lamina of all the vessels with schematic representation of the observation depth in two-photon microscopy (cortical layers I to III) and the observation depth in the immunohistochemistry studies (whole cerebral cortex).

2.4. Histology and immunohistochemistry

2.4.1. Slice preparation. At different timepoints post irradiation (48 h, one week and one month; three and six months for gliosis studies), animals (n = 5 per timepoint, except at six months: n = 4) were sacrificed and the brains were excised and frozen in isopentane at 193 K. Sagittal slices of thickness 10 µm were cut on a cryotome (Microm HM560).

2.4.2. Fluorescence microscopy. Slices were observed on a Nikon epifluorescence microscope (type Eclipse E600) equipped with a digital colour camera (Olympus, Color View II) and *analySIS* software (version 5, Soft Imaging System, Olympus, Munster).

2.4.3. Immunohistochemistry. Briefly, sections were fixed in a solution of paraformaldehyde (4%) and then permeabilized with a lysis buffer: sucrose 300 m*M*, $MgCl_2$ 3 m*M*, Tris 20 m*M*, NaCl 50 m*M* and Triton 0.5%. They were incubated overnight at 277 K with the primary antibody in PBS-BSA 3%. Finally, sections were incubated for 90 min at room temperature with the secondary antibody in PBS-BSA 3%. Slices were mounted with a mounting medium (Biomeda, Foster City) containing Hoechst 33342 (2 µg ml^{-1}).

The following primary antibodies were used: goat anti-collagen IV (1/100, Southern Biotech); goat anti-GFAP (1/100, Southern Biotech); rabbit anti-GFAP (1/100, DAKO); mouse anti-NeuN (1/100, Chemicon). The secondary antibodies used were TRITC conjugated donkey anti-goat (1/100, Jackson Immunoresearch); FITC conjugated donkey anti-rabbit (1/100, Jackson Immunoresearch); FITC conjugated donkey anti-mouse (1/100, Jackson Immunoresearch).

2.4.4. Vascular parameters. Vascular parameters were estimated using a home-made *ImageJ* macro. Digitized images (2080 × 1544 pixels) of collagen IV immuno-labelled slices were processed as follows: (i) automated binarization with threshold filter; (ii) removal of structures smaller than or equal to 2 pixels, and (iii) closing and filling of open vascular structures. Each binary picture was compared with the original one to verify the accuracy of the image processing. Then,

vascular density (number mm^{-2}) and vascular surface fraction (vascular area/sample area, %) were estimated.

3. Results

3.1. BBB permeability

In healthy animals, the two dyes (4 kDa FITC-dextran and 70 kDa RhodamineB-dextran) remained intravascular; no leakage into brain parenchyma was detected (Figs. 3A–3C). After mechanical BBB disruption, the 70 kDa RhodamineB-dextran molecules remained intravascular (Fig. 3D) while the 4 kDa FITC-dextran molecules leaked out into brain tissue (Fig. 3E). Cells appeared as dark spots surrounded by the 4 kDa FITC-dextran, as this dye does not cross cell membranes (Fig. 3F, white arrows).

Irradiated animals were observed 48 h (Figs. 3G–3I), one week (Figs. 3J–3L) and one month (Figs. 3M–3O) after irradiation. Both dyes remained intravascular and no leakage into brain parenchyma was observed between 48 h and one month after irradiation. The irradiation seemed not to disrupt BBB for molecules with a molecular weight of 4 kDa and above. Tridimensional reconstruction using the stack of images collected for the BBB permeability measurements revealed that there were no disruptions in the vascular network of the irradiated cortex and that all vessels stayed functional (data not shown).

3.2. Vascular parameters

After the intravital studies, brains were removed and vascular parameters were estimated in the irradiated volume using quantitative immunohistochemistry of collagen type IV staining of the basal lamina of all brain vessels. Vascular density and vascular surface fraction were estimated at 48 h, one week and one month after the irradiation. No modifications in vascular density and vascular surface area were observed in the cortex of irradiated animals (Table 1).

3.3. Effects on brain parenchyma

Gliosis, which can be described as an increase in the astrocyte population in damaged areas of the central nervous system, was assessed using immuno-labelling against the glial fibrillary acidic protein (GFAP). Such an increase was found neither in the short term (48 h to one month) nor in the long term (three and six months) after the irradiation (Fig. 4).

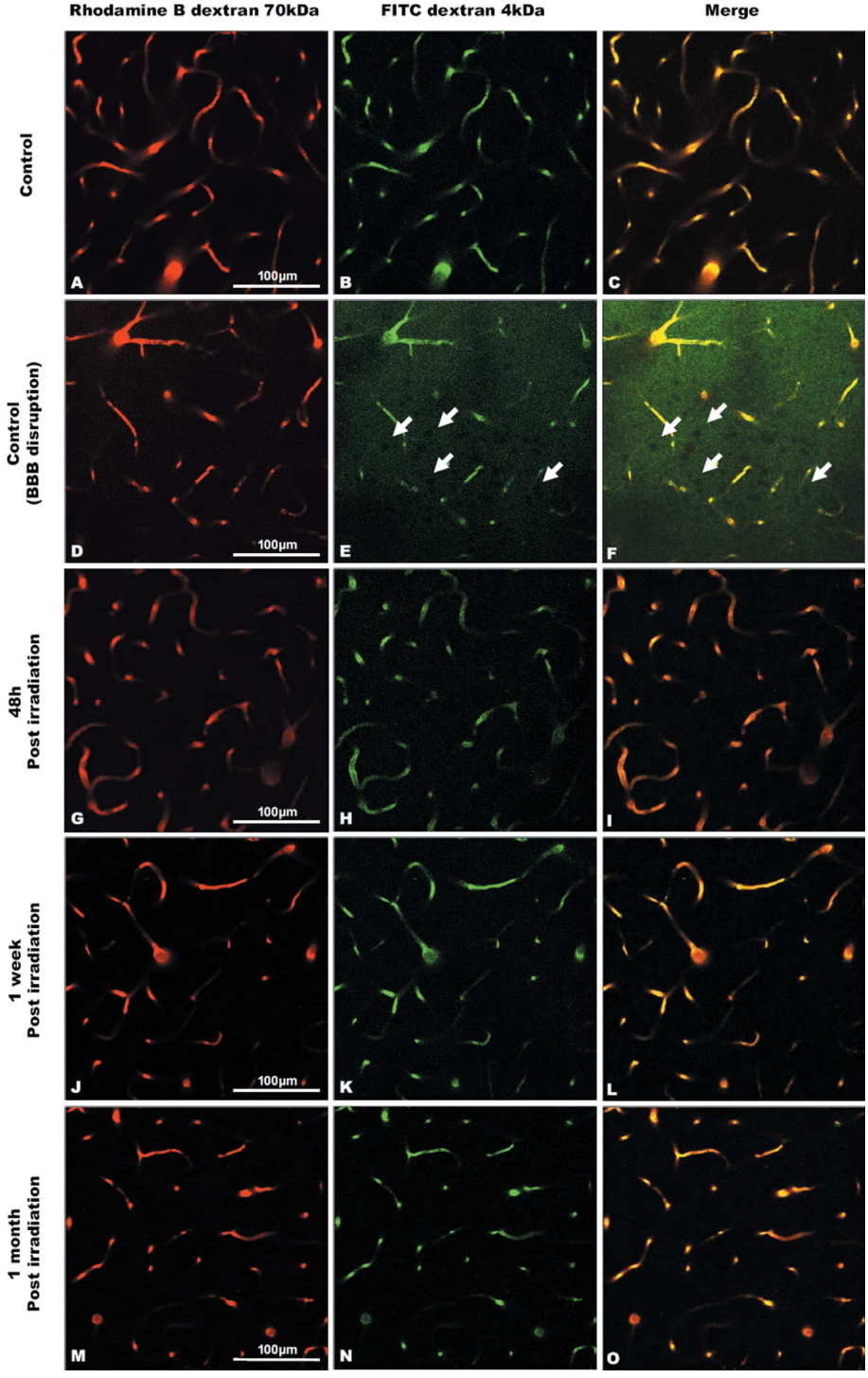

Figure 3
BBB permeability. Two-photon fluorescence microscopy images of RhodamineB-dextran 70 kDa (column I), FITC-dextran 4 kDa (column II) and merge of the two images (column III). Images were acquired at 150 µm below the dura in a healthy mouse (A–C); in a mechanically BBB induced disruption model (D–F); 48 h post irradiation (G–I); one week post irradiation (J–L) and one month post irradiation (M–O). Note the black holes (arrows, E–F) which are cells not labelled by the extravasated dye.

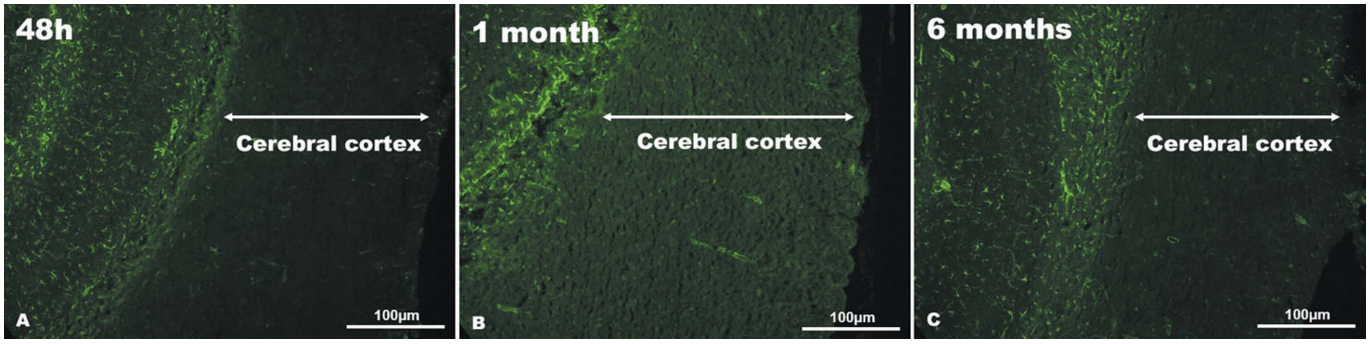

Figure 4
Gliosis. Immuno-labelling of GFAP on brain sections at 48 h (A), one month (B) and six months (C) after the irradiation.

Table 1
Evolution of vascular density and of the vascular surface fraction at different delays post irradiation (48 h to one month); $n = 5$ mice per delay.

Delay post irradiation	Vascular density (vessels mm^{-2})	Vascular surface fraction (%)
Control	339 ± 31	4.3 ± 0.6
48 h	343 ± 30	3.9 ± 0.5
One week	341 ± 37	3.9 ± 0.6
One month	344 ± 34	3.9 ± 0.6

Slices from irradiated cerebral cortex that had been stained with hematoxylin/eosin or with the NeuN neuronal marker did not reveal a different staining than corresponding slices from control animals (data not shown). Finally, one year survival observations were realised on four irradiated mice which stayed alive and exhibited normal motor function.

4. Discussion

Two different imaging modalities were used to assess the effects of synchrotron irradiation on brain microvasculature. Intravital two-photon imaging was used to measure BBB permeability to two different dyes but brain tissue penetration depth of this technique is limited to approximately 300 µm in adult mice. Therefore, quantitative immunohistochemistry after collagen IV staining of the basal lamina of all vessels was also applied to estimate the microvascular parameters at larger depths. Finally, the possible apparition of gliosis in brain tissue was examined using immunohistochemistry.

No extravasation of the two fluorescent dyes was observed after tomographic synchrotron irradiation applied in accordance with the PAT-Plat protocol (dose of 15 Gy and energy of 79 keV; no injection of cisplatin). Thus, it appears that the BBB remains impermeable to molecules with a molecular weight equal to or beyond 4 kDa. BBB disruption has often been reported, however, as a side effect of radiotherapy (van Vulpen *et al.*, 2002). Comparing results from studies on the effects of radiotherapy on BBB permeability may be difficult given that (i) radiosensitivities differ among animal species; (ii) dose, dose delivery and X-ray energy may vary considerably among studies; and (iii) BBB breakdown may be assessed using various methods, such as radiography of diffusible radioactive agents, MRI, immunohistochemistry and methotrexate (van Vulpen *et al.*, 2002). In the following, we therefore compare our results with studies performed on small rodent models using comparable techniques to assess BBB leakage, that is to say, techniques which allow the observation of leakage of dyes through the BBB on a microscopic scale.

Nakata *et al.* (1995) applied single doses of 20 Gy and 40 Gy in rat brains. They measured extravasation of serum components using immunohistochemistry with an antibody against serum albumin. Breakdown of the BBB was observed, for both doses, at already one day post irradiation. Extravasation of serum albumin reached its maximum three days after irradiation and decreased until complete disappearance by day 30.

Yuan *et al.* (2003) used 20 Gy, 6 MV focal irradiation. They performed intravital fluorescence microscopy focused on pial vessels in rats and reported that the permeability to 4.4, 10.0, 38.2 and 70 kDa FITC-dextran molecules was increased 24 h after irradiation. In contrast, no extravasation of 150 kDa FITC dextran molecules was found.

A temporary increase in BBB permeability during the first days after a single 20 Gy irradiation in rats (Nakata *et al.*, 1995; Yuan *et al.*, 2003) was not found in our mice experiments that were irradiated at 15 Gy. The molecular weight of the FITC-dextran used in our study (70 kDa) is comparable with that of serum albumin [67 kDa (Sigma)]. Thus we would expect that both molecules would behave comparably. Further difficulties may result in the radiosensitivity of the BBB that may differ between mice and rats.

In another study, Yuan *et al.* (2006) used fractionated dose delivery in C57BR/6J mice (whole-brains irradiation; 40 Gy delivered in daily fractions of 2 Gy, five times a week). They reported an increase of BBB permeability at 40 Gy to 4.4 and 38.2 kDa FITC-dextran molecules occurring only 90 days after the start of the delivery of the fractionated dose. It seems that the BBB effects of 40 Gy fractionated radiotherapy appear later than those of a single 40 Gy dose [see earlier rat studies (Yuan *et al.*, 2003)]. Irradiation with a single 15 Gy dose in our study did not induce BBB permeability in between 48 h and one month after irradiation. Within this time span an increase in BBB permeability was observed in other single irradiation studies on rats at a higher dose of 20 Gy. Hence, 15 Gy seems to be an acceptable dose for healthy mice brain tissue.

Alteration of vascular parameters other than the BBB permeability may also lead to functional impairments (Brown *et al.*, 2007). Therefore, we measured changes in vascular density and surface over the whole irradiated volume. No modifications were observed during the first month after irradiation. These findings are in line with those from a study by Roth *et al.* (1999) showing unaffected vascular density in irradiated hamster muscles up to 30 days after a 10 Gy (6 MV) irradiation. However, it must be noted that another study by Ansari *et al.* (2007) has shown that irradiating one hemisphere of the C57BL mice brain (dose 20 Gy, 6 MV) results in changes in brain vascular density.

Gliosis is often reported as an important side effect of irradiation and may cause functional impairments (Akiyama *et al.*, 2001). In the study of Yuan *et al.* (2006) on mice, the number of GFAP positive cells had doubled at 60 days after onset of the fractionated radiotherapy. Gliosis was still present 180 days after the beginning of the treatment but no differences with an unirradiated control were observed at 30 days. More interestingly, gliosis was located in the cerebral cortex, but no significant increase in the number of GFAP positive cells was seen in the hippocampus. Chiang *et al.* (1993) have also performed whole brain irradiation in mice. Increases in the GFAP level between 120 and 180 days after a single irradiation dose of 20 and 45 Gy were found. No increases were observed for doses of 2 and 8 Gy. More recently, Hwang *et al.* (2006) have shown that whole-brain irradiation with a dose of 15 Gy (6 MV) induced a significant increase in the number of GFAP positive cells in the rat brain cortex at 6 h post-irradiation and a further increase at 24 h.

We did not detect gliosis in the irradiated cortex either in the short term (48 h, one week, one month) or in the long term (three and six months) post irradiation. Immuno-labelling was carried out using two different antibodies from different suppliers. Converging results were obtained. The absence of gliosis in healthy brain tissue is important information in the perspective of the setting up of clinical trials, as gliosis is often related to functional impairments (Akiyama *et al.*, 2001; Eijkenboom *et al.*, 2004).

It is not easy to define the limit between radiotolerance and the apparition of side effects; as explained before, this limit may vary considering the species, the dose, the dose fractionation, the energy and the irradiated volume. This could explain the discrepancies between our results and some of the other studies. One of the explanations of the absence of side effects with our protocol could be the small volume that was irradiated in the parietal cortex (approximately 1.75 mm^3) which may facilitate repair processes by surrounding normal tissues.

5. Conclusions

Photoactivation therapy of cisplatin using synchrotron X-rays is a promising therapy for treatment of GBM. Curative effects on rats bearing the F98 glioma were reported in one-third of the animals treated with a dose of 15 Gy, an irradiation energy tuned about the *K*-edge of the platinum and an intratumoral injection of 3 µg of cisplatin (Biston *et al.*, 2004). In the present study, we have shown that irradiating with a beam identical to that applied in the PAT-Plat protocol did not cause severe damage to normal brain vasculature or gliosis, within one month post irradiation. The absence of side effects in the short term following the irradiation is of the foremost importance as healthy areas will have to be irradiated if we want to cover the whole tumoral volume. These results are particularly encouraging in view of the forthcoming phase-1 clinical trials at the ESRF.

The authors warmly thank all colleagues of the medical beamline at the European Synchrotron Radiation Facility. They are also very grateful to Dr Samuel Valable and Benjamin Lemasson for providing the *ImageJ* macro. Helpful discussion with Professor François Estève is acknowledged. CR is recipient from a grant of the French Ministry of Education and Research.

References

Adam, J., Elleaume, H., Joubert, A., Biston, M.-C., Charvet, A., Balosso, J., Le Bas, J. & Estève, F. (2003). *Int. J. Radiat. Oncol. Biol. Phys.* **57**, 1413–1426.
Adam, J.-F., Joubert, A., Biston, M.-C., Charvet, A.-M., Peoc'h, M., Le Bas, J.-F., Balosso, J., Esteve, F. & Elleaume, H. (2006). *Int. J. Radiat. Oncol. Biol. Phys.* **62**, 603–611.
Akiyama, K., Tanaka, R., Sato, M. & Takeda, N. (2001). *Neurol. Med. Chir. (Tokyo)*, **41**, 590–598.
Ansari, R., Gaber, M. W., Wang, B., Pattillo, C. B., Miyamoto, C. & Kiani, M. F. (2007). *Radiat. Res.* **167**, 80–86.
Behin, A., Hoang-Xuan, K., Carpentier, A. & Delattre, J.-Y. (2003). *Lancet*, **361**, 323–331.
Bernier, J., Hall, E. & Giaccia, A. (2004). *Nat. Rev. Cancer*, **4**, 737–747.
Biston, M.-C., Joubert, A., Adam, J.-F., Elleaume, H., Bohic, S., Charvet, A.-M., Esteve, F., Foray, N. & Balosso, J. (2004). *Cancer Res.* **64**, 2317–2323.
Brown, W., Blair, R., Moody, D., Thore, C., Ahmed, S., Robbins, M. & Wheeler, K. (2007). *J. Neurol. Sci.* **257**, 67–71.
Chiang, C., McBride, W. & Withers, H. (1993). *Radiother. Oncol.* **29**, 60–68.
DeAngelis, L. (2001). *N. Engl. J. Med.* **344**, 114–123.
DeAngelis, L., Delattre, J.-Y. & Posner, J. (1989). *Neurology*, **39**, 789–796.
Eijkenboom, M., Gerlach, I., Barker, A., Luiten, P. & van der Staay, F. (2004). *Neuroscience*, **124**, 523–533.
Greenlee, R., Murray, T., Bolden, S. & Wingo, P. (2000). *CA Cancer J. Clin.* **50**, 7–33.
Gurney, J. & Kadan-Lottick, N. (2001). *Curr. Opin. Oncol.* **13**, 160–166.
Helmchen, F. & Denk, W. (2005). *Nat. Methods*, **2**, 932–940.
Hwang, S.-Y., Jung, J.-S., Kim, T.-H., Lim, S.-J., Oh, E.-S., Kim, J.-Y., Ji, K.-A., Joe, E.-H., Cho, K.-H. & Han, I.-O. (2006). *Neurobiol. Dis.* **21**, 457–467.
König, K. (2000). *J. Microsc.* **200**, 83–104.
Mehta, M. & Khuntia, D. (2005). *Neurosurgery*, **57**, S4-33–S34-44.
Muldoon, L., Soussain, C., Jahnke, K., Johanson, C., Siegal, T., Smith, Q., Hall, W., Hynynen, K., Senter, P., Peereboom, D. & Neuwelt, E. (2007). *J. Clin. Oncol.* **25**, 2295–2305.
Nakata, H., Yoshimine, T., Murasawa, A., Kumura, E., Harada, K., Ushio, Y. & Hayakawa, T. (1995). *Acta Neurochir (Wien)*, **136**, 82–86.
Roman, D. & Sperduto, P. (1995). *Int. J. Radiat. Oncol. Biol. Phys.* **31**, 983–998.

Roth, N., Sontag, M. & Kiani, M. (1999). *Radiat. Res.* **151**, 270–277.
Rousseau, J., Boudou, C., Barth, R., Balosso, J., Esteve, F. & Elleaume, H. (2007). *Clin. Cancer Res.* **13**, 5195–5201.
Rousseau, J., Boudou, C., Esteve, F. & Elleaume, H. (2007). *Int. J. Radiat. Oncol. Biol. Phys.* **68**, 943–951.
Schenke-Layland, K., Riemann, I., Damour, O., Stock, U. A. & Konïg, K. (2006). *Adv. Drug Deliv. Rev.* **58**, 878–896.
Schultheiss, T., Kun, L., Ang, K. & Stephens, L. (1995). *Int. J. Radiat. Oncol. Biol. Phys.* **31**, 1093–1112.
Stupp, R. *et al.* (2005). *N. Engl. J. Med.* **352**, 987–996.
Turchi, J. J., Henkels, K. M. & Zhou, Y. (2000). *Nucleic Acids Res.* **28**, 4634–4641.
Van Tassel, P., Bruner, J., Maor, M., Leeds, N., Gleason, M., Alfred Yung, W. & Levin, V. (1995). *Am. J. Neuroradiol.* **16**, 715–726.
Vulpen, M. van, Kal, H., Taphoorn, H. & el Sharouni, S. (2002). *Oncol. Rep.* **9**, 683–688.
Yuan, H., Waleed Gaber, M., Boyd, K., Wilson, C., Kiani, M. & Merchant, T. (2006). *Int. J. Radiat. Oncol. Biol. Phys.* **66**, 860–866.
Yuan, H., Waleed Gaber, M., McColgan, T., Naimark, M., Kiani, M. & Merchant, T. (2003). *Brain Res.* **969**, 59–69.